OPTIMAL FLARE AND LANDING OF A HELICOPTER IN TAIL ROTOR FAILURE

Hikmet Berkay Ayık, Turkish Aerospace, Ankara, Türkiye
Yusuf Onur Arslan, Turkish Aerospace, Ankara, Türkiye

Abstract

The main goal of this study is to find an optimal flare and landing maneuver for a helicopter that has been stabilized and has been brought into autorotation trim after experiencing a tail rotor failure. In this work, the previous studies of the authors are concluded by covering a landing scenario, starting from stable autorotation and ending with a safe landing. The trajectory generation process utilizes linearized models from the default FLIGHTLAB helicopter model. The obtained trajectories are then fed into a tracking controller, and nonlinear simulations are performed in FLIGHTLAB environment. The investigation is repeated for different types of tail rotor failure.

1. NOTATION

Symbols

X	State Vector
U	Input Vector
u, v, w	Velocities in Body Axes, $[\mathrm{ft}/s]$
p, q, r	Roll, Pitch and Yaw Rates, $[°/s]$
x_i, y_i, z_i	Positions in Inertial Frame, $[\mathrm{ft}]$
β	Sideslip Angle, $[°]$
Ω	Main Rotor Rotation Speed, $[\%]$
$\dot{\Omega}$	Main Rotor Acceleration, $[\%/s]$
ϕ	Roll Angle, $[°]$
θ	Pitch Angle, $[°]$
ψ	Yaw Angle, $[°]$
$\delta_{\mathrm{col}}, \delta_{\mathrm{lon}}, \delta_{\mathrm{lat}}, \delta_{\mathrm{ped}}$	Control Inputs, $[\%]$

Acronyms:

TRF	Tail Rotor Failure
MR	Main Rotor
TR	Tail Rotor
NR	Main Rotor Speed

Copyright Statement

The authors confirm that they, and/or their company or organization, hold copyright on all of the original material included in this paper. The authors also confirm that they have obtained permission, from the copyright holder of any third-party material included in this paper, to publish it as part of their paper. The authors confirm that they give permission, or have obtained permission from the copyright holder of this paper, for the publication and distribution of this paper as part of the ERF proceedings or as individual offprints from the proceedings and for inclusion in a freely accessible web-based repository.

2. INTRODUCTION

One of the most critical emergency scenarios for conventional single main rotor helicopters during flight is tail rotor failure. A tail rotor failure is defined as the complete or partial loss of tail rotor effectiveness and directional control. The tail rotor plays a vital role in yaw stability and control by counteracting the torque generated by the main rotor. Another contributor to the anti-torque generation is the vertical fin, although it is not as effective in low-speed flight conditions. Different kinds of tail rotor failures might occur during a flight, ranging from pedal jamming to complete loss of the tail rotor. Since anti-torque sources are scarce, a loss of tail rotor control could lead to catastrophic accidents, especially in low-speed flight regimes. Tail rotor loss-related accidents have occurred both historically and in recent years, with two examples cited in References 1 and 2, where a Robinson R22 and a Bell 505, respectively, experienced different tail rotor failure incidents, fortunately resulting in no casualties. In the case of a tail rotor failure emergency, entering an immediate autorotation is the standard procedure for recovery. By maintaining the helicopter in stable condition, a safe landing site should be reached as soon as possible. Upon reaching a certain altitude, an autorotative flare maneuver is to be performed to reduce the descent rate, cushion the rotorcraft, and ensure a safe landing. This procedure is explained in detail in Reference 3.

Recently, new studies were included in the literature in helicopter emergency scenarios. Saetti's study (Ref. 4) focuses on autorotative flare maneuver in a fully autonomous helicopter. The study combines rapid path generation with model-based control. The path generation is performed using a Tau theory and the flare trajectory is tracked by a nonlinear dynamic inversion-based controller. The results of this study indicated that the proposed approach can successfully simulate an autorotative maneuver for UH-60 helicopter.

Reference 5 investigates the autorotation of small-scale helicopters in case of engine failure. A model-based design approach is used to examine the steady descent autorotation and a possible flare maneuver. An offline autorotation trajectory is obtained and followed by a closed-loop controller. Their approach resulted in successful flare maneuvers in terms of reducing the touch-down velocities to acceptable limits. The study also analyzes the maneuver's sensitivity to initial velocity and altitude by simulating different initial conditions.

Fattizzo (Ref. 6) focuses on automatic helicopter autorotation and landing after the engine failure. An autorotation maneuver is designed based on initial condition constraints. Furthermore, a nonlinear dynamic inversion-based controller is developed to perform autorotation and flare. The results showed that the desired velocities and attitude at touch-down are achievable.

In previous studies conducted by the authors, the flight characteristics of a rotorcraft experiencing tail rotor failure were investigated step by step and in depth. In Reference 7, a rotorcraft in stable flight condition with a failed tail rotor was investigated. The trajectories that guide the rotorcraft from a steady flight condition to a desired flight condition are successfully generated. The analyses are completed by implementing a set of linear models into a primitive model-stitching architecture. In Reference 8, new trajectories are generated for new scenarios, and a controller is implemented into the system. Using this controller, tracking performance over generated trajectories was studied. The states are tracked by an LQI controller, and the position is tracked by an inversion-based controller. This study also used the same method for the trajectory generation process as in the previous study. Trajectory tracking is accomplished by connecting Simulink and FLIGHTLAB environments and feeding the trajectory into the simulation. The main focus of Reference 9 is the stabilization of the rotorcraft after the tail rotor failure. The effects of variable main rotor speed are investigated. For that study, an advanced stitched model is created by using linear models obtained from FLIGHTLAB, and using the methods explained by Tischler (Ref. 10.) That model is capable of trimming the rotorcraft at the required flight condition and continuous full flight envelope simulations. The model is used to obtain stabilization trajectories after the instant of failure and the trajectories for the transition between the flight conditions. The trajectories obtained were again followed by a tracking controller and their validity is evaluated.

The main objective of this study is to complete the tail rotor failure emergency procedure by incorporating an autorotative flare maneuver that enables a safe landing. After reaching a stable autorotation trim following a tail rotor failure, trajectories governing the flare and landing phases are obtained for three different failure and controllability scenarios. The flight paths are generated using an open-source trajectory optimization tool, OptimTraj (Ref. 11). The trajectory optimization problem is defined by an objective function, path constraints, and system dynamics. The problem is solved by OptimTraj, which uses direct collocation method. The linear models are obtained from generic FLIGHTLAB model and are used for path generation. The landing maneuvers are obtained for different tail rotor failure scenarios, including pedal jamming and hard-over condition of the tail rotor actuator. The effect of the ability to directly control the main rotor speed is also investigated. Two helicopter models with different engine dynamics are utilized. One of the models includes an ideal engine model and has control in rate of main rotor speed, while the second model has a simple engine model; hence, the main rotor speed changes due to engine dynamics. The resulting trajectories are used in nonlinear simulations on FLIGHTLAB environment. The FLIGHTLAB Run-Time model is integrated with SIMULINK for this purpose. An LQI controller is employed to track the previously obtained states. The constraints defining the operational limits for a safe landing are adopted from Reference 12.

Methodology

2.1. Helicopter Model

Generic nonlinear FLIGHTLAB helicopter model based on Sikorsky UH-60A is utilized in this study to provide helicopter dynamics. The base configuration with 7380 kg total weight, 9.144 m x CG, neutral y CG and 6.401 m z CG is used.

The previous studies incorporated stitched model architecture for the trajectory generation process. However, the model-stitching approach was deemed unsuitable for this study, since the only reasonable trim point from which a linear model could be extracted was the initial condition. The highly transient nature of the flare maneuver does not allow for the identification of another trim point to be used in the stitched model. Therefore, the linear models representing the states and dynamics at the beginning of autorotative flare maneuver formed the basis for helicopter dynamics in this study.

The trim points and corresponding linear models are found by trimming and linearizing the nonlinear FLIGHTLAB model including the tail rotor failure at the flight scenarios of interest. The trajectory optimization process utilizes the linear models provided by the linearization process.

In order to reduce the model complexity, the horizontal tail controller, pitch bias controller and SAS are switched off. The mechanical mixing of the pilot controls is also eliminated for the same reason.

The study also investigates the effect of the main rotor speed control during the flare maneuver. Therefore, two nonlinear models, one with the ideal engine and the one with the simple engine, are utilized for the analyses. In the nonlinear model with ideal engine, the main rotor speed (NR) remains constant at 100%, regardless of the torque requirement during any maneuver. However, the rate of NR is added into the pilot controls in order to investigate its benefit for the helicopter in tail rotor failure. Equations (1) and (2) represents the states and the controls of the linearized form of the nonlinear model with the ideal engine.

(1) $$X = [\Omega \quad \phi \quad \theta \quad u \quad v \quad w \quad p \quad q \quad r]^T$$

(2) $$U = \left[\delta_{col} \quad \delta_{lon} \quad \delta_{lat} \quad \delta_{ped} \quad \dot{\Omega}\right]^T$$

In the nonlinear model with the simple engine, the main rotor speed is not added into the pilot controls and changes only depending on torque requirement during the maneuver. The clutch mechanism is also included in this model. The state and input vectors for linearized form of this model are given in Equations (3) and (4).

(3) $$X = [\Omega \quad \phi \quad \theta \quad u \quad v \quad w \quad p \quad q \quad r]^T$$

(4) $$U = [\delta_{col} \quad \delta_{lon} \quad \delta_{lat} \quad \delta_{ped}]^T$$

FLIGHTLAB Run-time System allows the use of the generic nonlinear model for tracking simulations. A black-box model that can be interfaced with external systems called FCM model is generated by using FLIGHTLAB SIMPHONY module. An interface script to drive the FCM model and regulate the input-output signals is prepared. The script is used to transfer data between SIMULINK and SIMPHONY via UDP communication protocol.

2.2. Trajectory Optimization

The flight paths are generated using OptimTraj (Ref. 11). The optimization problem is constrained by the terminal states of the helicopter in tail rotor failure condition, as well as an objective function and bounds on states and controls. Each scenario begins in autorotation with a certain tail rotor failure and aims to land within the defined landing criterion.

The optimization tool computes the optimal state and control trajectories that navigate the helicopter from the maneuver starting condition, 80 kt autorotation since it is the suggested autorotation speed for conventional helicopters, to the landing conditions while the failure persists.

The minimum control input objective function is implemented for state navigation. The reason for this decision is that a helicopter with a tail rotor failure in a steady flight condition is prone to be unstable; thus, inputs must be delicate and accurate. The cost function for minimum input is given in Equation (5).

(5) $$\min \int_{t_0}^{t_F} u^2 dt$$

To realistically perform the maneuver, a path constraint is defined for altitude. For the study, it is decided that the initial altitude of the helicopter is 100 ft, and the trajectory generation shall be completed within this range. The corresponding function is defined in Equation (6).

(6) $$c_{eq} = zi - 100$$

Provided in UH60 Operator Manual (Reference 12), forward touch-down speed and descent rate limitations for landing are defined in Equation (7). Although no sideslip limitation is given in Operator Manual, the lack of directional control requires a threshold on sideslip angle at touch-down as well. The success of projected landings is evaluated according to these conditions.

$$c = \begin{bmatrix} Ground\,Speed & < & 60\,kt \\ Vario & < & 540\,fpm \\ Sideslip & < & 15° \end{bmatrix} \quad (7)$$

The optimum paths from steady autorotation to landing with tail rotor failure are obtained from the offline process and given as a reference to the controller for tracking.

2.3. Trajectory Tracking

A linear quadratic regulator with integral action is implemented for tracking the helicopter states in nonlinear simulations. A detailed explanation of the process can be found in Reference 8 since trajectory tracking is the main focus of that study.

The state paths that guide the helicopter to landing condition are given as a reference to the tracking controller and nonlinear simulations are performed to investigate the accuracy of the obtained trajectories.

The weighting matrix for the state error, *Q*, and the weighting matrix for the input effort, *R*, are selected according to whether the rate of main rotor speed control is present or not. For the cases in which the main rotor speed rate is among the pilot controls, the states for tracking are given in Equation (8). Due to the nature of the flare maneuver, pitch angle and body z-velocity are the most essential states that determine the success of the maneuver. The lateral dynamics and sideslip angle are regulated by tracking roll angle and main rotor speed.

$$x = [\Omega \quad \phi \quad \theta \quad w]^T \quad (8)$$

If the control of main rotor speed rate is not included in pilot controls, the tracked states are selected as provided in Equation (9). The lateral control is provided by tracking body y-velocity instead of roll angle and main rotor speed. Although roll angle and body y-velocity are interchangeable in lateral control, selecting y-velocity improved the controller performance for this case. Since the maneuver is governed by body states, and the rate of main rotor speed is not a control, main rotor speed is selected as the state to be eliminated to preserve the rank of the under-actuated system.

$$x = [\theta \quad v \quad w]^T \quad (9)$$

3. RESULTS AND DISCUSSION

In this work, trajectories that guide a conventional helicopter with tail rotor failure from autorotation to a safe landing condition are generated. The main objective is to obtain suitable trajectories, verify them through nonlinear simulations using a tracking controller, and finally evaluate touch-down performance under the tail rotor failure condition.

The impact of direct control over main rotor speed is also investigated. Previous studies have demonstrated that it is possible to stabilize the helicopter after a tail rotor failure and bring it into autorotation trim. Therefore, in this study, the trajectories are generated starting from a steady autorotation condition.

For trajectory optimization, the main rotor speed is bounded between 88% and 112%. Although the selected bounds slightly exceed the operational limits of many conventional helicopters, considering the nature of the maneuver, any decision that could offer an advantage in an emergency situation is deemed acceptable. States are loosely bounded during the maneuver, as the flare maneuver is highly nonlinear and dynamic, requiring aggressive control inputs and resulting in highly variable velocities and attitudes. The target terminal states are determined to ensure a safe landing upon completion of the maneuver. Time required to reach the desired terminal conditions are also found by OptimTraj, and simulations are conducted for that exact duration. Ground contact is not in the scope of this work, and it is assumed that when the terminal states are achieved, a safe touch-down can be performed easily.

The specific flight scenarios examined are summarized in Table 1. Each scenario is analyzed using two models, one with the ideal engine and the other with the simple engine.

Table 1: Investigated Flight Scenarios

Scenario	From	To
1	80 kt Autorotation Complete Loss of TR	Landing
2	80 kt Autorotation Pedal Jamming	Landing
3	80 kt Autorotation TR Actuator Hard-Over	Landing

For Scenario 1, the helicopter model is trimmed with complete tail rotor loss. Scenario 2 utilized a linear model with pedal jamming at 30%. Note that 0% pedal corresponds to maximum TR thrust. Scenario 3 assumes the hard-over of the tail rotor actuator, forcing the actuator to the maximum thrust position. The helicopter model could not be stabilized at 0% pedal. Therefore, the analyses are conducted for 5% pedal.

Trajectory tracking process is completed only for Scenario 1 with both models. As the method yielded consistent and sufficient results in previous studies and in Scenario 1, no further validation is considered as necessary. Therefore, the nonlinear simulations are not performed for Scenarios 2 and 3.

The figures for each scenario, with and without main rotor speed control, are presented in the corresponding appendix. Solid black lines illustrate the simulation results while dashed black lines indicate OptimTraj estimations. Red dashed lines in state plots are used to highlight the tracked states in simulations. The solid red lines in landing parameters indicate the allowed limits for landing.

3.1. Scenario 1 – Complete Loss of Tail Rotor

The first scenario simulates the autorotative flare and landing under complete loss of the tail rotor condition. Directional control via pedal input is not possible as tail rotor produces no thrust. Both trajectory optimization and tracking simulation are conducted for this scenario.

Firstly, the analysis is performed using the ideal engine model. The control inputs that initiate the flare maneuver can be seen in Figure 1. The optimized trajectory requires variation in main rotor speed; therefore, the controller adjusts the NR rate accordingly. As observed in Figure 2, although NR is independent of helicopter dynamics in the ideal engine model, the controller increases it to utilize the kinetic energy of the rotor, as in a typical flare maneuver. Figure 3 illustrates the Euler angles of the helicopter. The pitch angle increases and peaks at 25° until the resting state is achieved. After the rest, NR is reduced, and collective is increased to perform the touch-down. Figure 4 shows that although the maneuver is estimated to be completed within 100 ft, the nonlinear simulation requires 125 ft altitude to complete the flare and landing. According to Figure 5, although the sideslip angle is out of the safe landing limitation at the end of the simulation, there is a time interval during which all the landing criterion are satisfied. However, as the simulation is conducted for the exact final time found by OptimTraj, the nonlinear dynamics cause the trajectory and simulation to differ.

Secondly, the scenario is repeated with the simple engine model. As shown in Figure 6, input profiles are similar to the first analysis. While the longitudinal dynamics resemble the analysis with the ideal engine, lateral dynamics behave differently as illustrated in Figure 7 and Figure 8. The reason for this is that in the simple engine model, the clutch disengages and removes the need for anti-torque. Therefore, the heading is not affected by NR change. Figure 9 shows that the execution of the maneuver is completed within 125 ft altitude, exceeding the OptimTraj estimation of 100 ft. As provided in Figure 10, all parameters regarding the landing safety are in allowable range, indicating a safe landing.

The estimated trajectories for both models exhibit the characteristics of a standard flare maneuver, and simulation results validate their feasibility. The trajectories and nonlinear simulation results are mostly in good agreement, although a slight delay is noticeable in state tracking. Although only the states are tracked by the controller, pilot input profiles show strong similarity to the estimated controls. The slight differences between the optimized trajectories and the simulations are due to the nonlinear dynamics of the helicopter.

3.2. Scenario 2 – Pedal Jamming

The second scenario simulates the landing after autorotation with pedal jamming. The pedal is jammed at 30% during the simulations. For this scenario, only trajectory optimization is completed, and nonlinear simulations are not performed.

The optimized pilot control inputs for the ideal engine model are presented in Figure 11. Figure 12 shows that only a modest increase in main rotor speed is utilized, unlike a real flare maneuver. The pitch angle increases, and the helicopter rolls left as illustrated in Figure 13 to decelerate and reach resting state. Uncontrollable tail rotor thrust combined with the torque from the engine results in deviation from initial heading. As seen in Figure 14, although the rotorcraft does not come to a complete stop, it is brought into a landing attitude through collective and cyclic inputs. The optimized trajectory increases NR to generate anti-torque and control heading as the helicopter nears ground. The descent rate, ground speed and sideslip at the touch-down are all within the acceptable limits as illustrated in Figure 15. The maneuver is estimated to be completed in 100 ft descent.

The trajectory with the simple engine model utilizes similar pilot control inputs as the ideal engine model analysis as shown in Figure 16, with the exception of NR. Figure 17 and Figure 18 illustrate that NR and pitch angle increase as in a real flare maneuver and the kinetic energy of rotor is utilized. In this analysis, NR is used to convert the rotor's kinetic energy, rather than to enhance directional control as in the ideal engine model analysis. Roll angle decreases until the resting phase, which can be seen in Figure 19, and then sharply increases, reducing lateral speed and sideslip as shown in Figure 20. Towards the end of the maneuver, abrupt inputs are given to collective, longitudinal cyclic and lateral cyclic to reduce NR and recover to an appropriate attitude for landing. At the instant of touch-down, all related parameters are well within the limitations, indicating a safe landing. Compared to the ideal engine model, the simple engine model requires more pilot input in lateral cyclic and results in a higher sideslip angle at touch-down, suggesting that the ability to control main rotor speed improves directional control authority.

3.3. Scenario 3 – Tail Rotor Actuator Hard-Over

The final scenario covers the tail rotor actuator hard-over. The tail rotor actuator is assumed to have failed and jammed at 5% pedal position. The tail rotor is providing maximum uncommanded thrust throughout the maneuver. Optimum trajectories are obtained but nonlinear simulations are not conducted for this scenario.

Control input estimations for this scenario with the ideal engine model are presented in Figure 21. NR is increased while collective and cyclic inputs are used to initiate a maneuver similar to flare in both pitch and roll axis. As illustrated in Figure 22 and Figure 23, NR is increased; pitch angle peaked at 25° while the helicopter rolls up to 20° left. Heading diverges from the trim as torque requirement changes and NR increases. As the helicopter approaches to the ground as seen in Figure 24, although there is no full rest, NR is decreased to control the heading and sideslip while roll and pitch angles are brought to a more suitable attitude for landing. Figure 25 indicates that at the instant of touch-down, all related parameters are within acceptable range. However, the sideslip angle being exactly 15° might pose some risks for landing.

OptimTraj estimation of control inputs for this scenario with the simple engine model is given in Figure 26. Optimized input profiles are different than the inputs for the ideal engine model trajectory, as extreme and abrupt inputs are observed throughout this analysis. As presented in Figure 27 and Figure 28, NR could not be increased and roll angles up to 40° are reached. Pitch up attitude required for a flare maneuver could not be maintained as roll angle change drastically throughout the maneuver. At the end of the resting state, a small increase in altitude is observed in Figure 29, and the landing is initiated afterwards. As can be seen in Figure 30, the ground speed at touch-down is exactly 60 kt and the descent rate is just below the limitation. Combining these with 30° sideslip, which is above the limitation, it can be said that a safe landing is not ensured.

This scenario underlines the importance of main rotor speed control in ensuring a manageable flare and landing. While a safe landing solution cannot be found with only conventional pilot controls, the optimized trajectory to a safe landing can be generated when the rate of main rotor speed is included in pilot controls. When rotor speed is directly controlled, it becomes possible to adjust the helicopter's attitude, velocity, and descent rate smoothly, eliminating the need for extreme control inputs or abrupt attitude changes.

4. CONCLUSION

The study investigates three tail rotor failure scenarios. Each scenario is evaluated with two models, one that has a direct control over main rotor speed and the other in which the main rotor speed is not among the controls. Findings suggest that helicopters can still execute a safe flare and landing maneuver under conditions such as total tail rotor loss, pedal jamming, or actuator hard-over. Based on the results, it can be stated that the failure that poses the greatest challenge is found to be hard-over of the tail rotor actuator.

Furthermore, having a direct control over the main rotor speed improves the directional control of the helicopter. In hard-over scenario, the helicopter could not land in the defined sideslip limitation if its main rotor speed is not controlled. When the direct control over the main rotor speed is implemented, landing conditions are satisfied.

A complete simulation covering the entire sequence from the tail rotor failure instant to touch-down, with a sophisticated controller and incorporating a ground interaction model and landing gear dynamics, would be a valuable addition to this study as future work.

Author contact:

Hikmet Berkay Ayık hikmetberkay.ayik1@tai.com.tr

Yusuf Onur Arslan yusufonur.arslan@tai.com.tr

5. APPENDIX

5.1. Appendix A: Scenario 1

5.1.1. With MR Speed Control

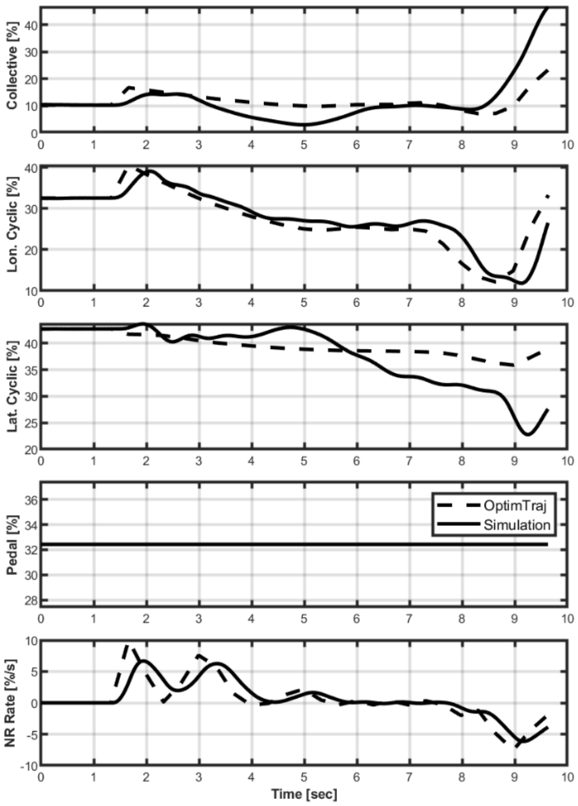

Figure 1. Pilot Controls, Complete Loss of TR with MR Speed Control

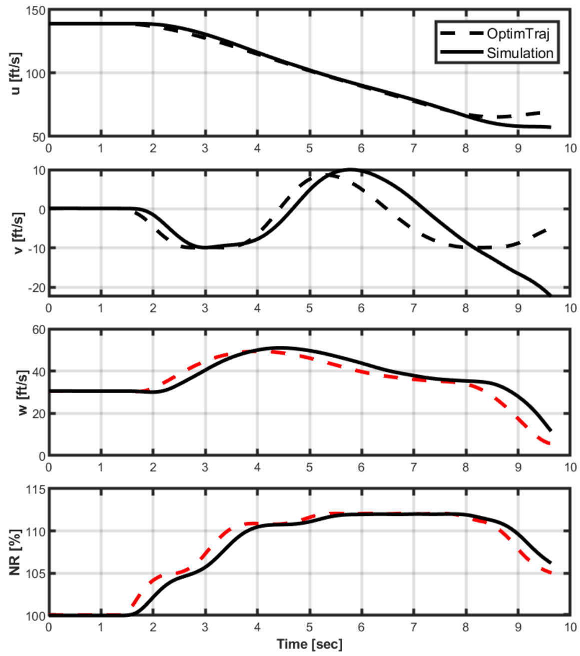

Figure 2. Body Velocities and NR, Complete Loss of TR with MR Speed Control

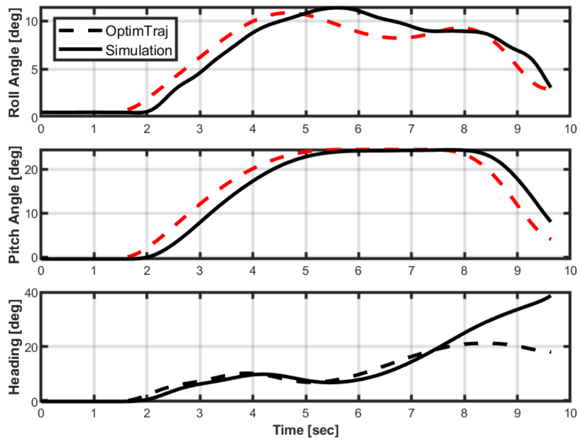

Figure 3. Euler Angles, Complete Loss of TR with MR Speed Control

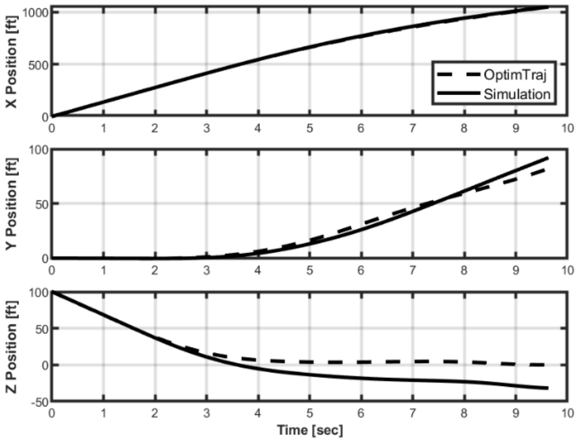

Figure 4. Inertial Positions, Complete Loss of TR with MR Speed Control

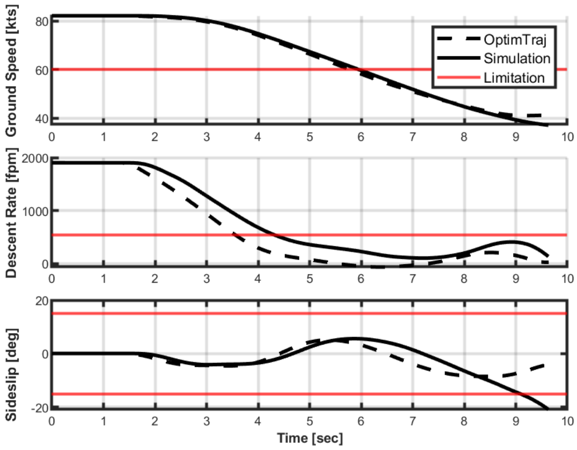

Figure 5. Landing Parameters, Complete Loss of TR with MR Speed Control

5.1.2.Without MR Speed Control

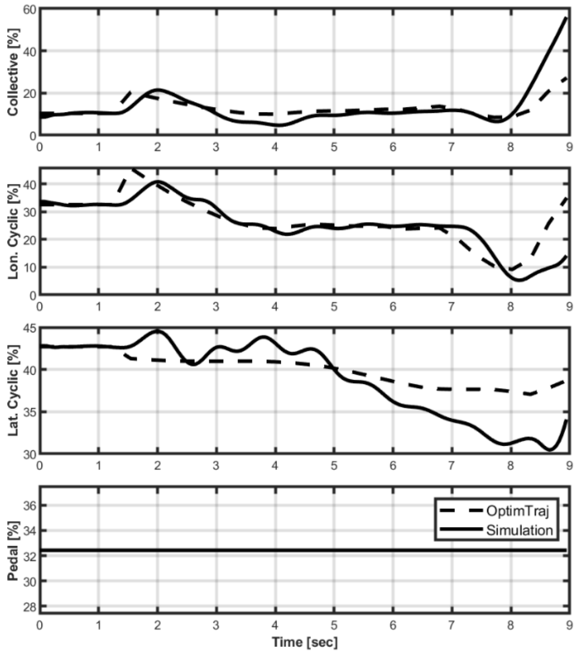

Figure 6. Controls, Complete Loss of TR without MR Speed Control

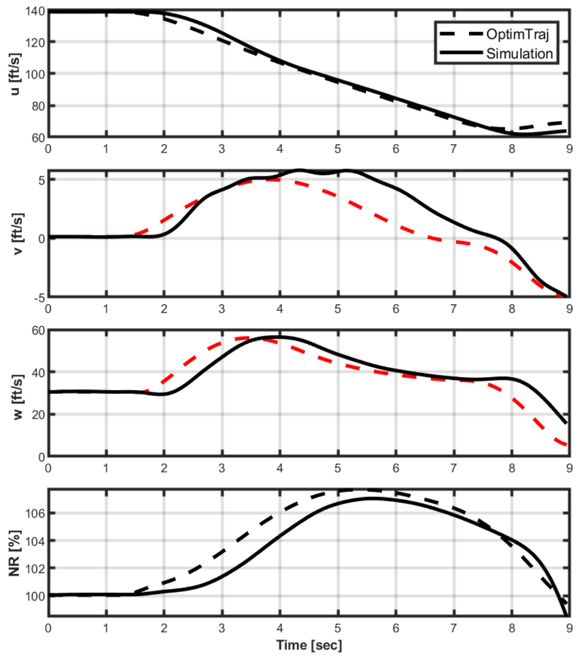

Figure 7. Body Velocities and MR Speed, Complete Loss of TR without MR Speed Control

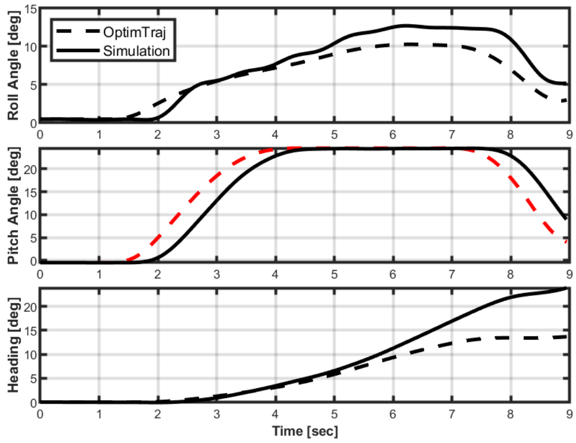

Figure 8, Euler Angles, Complete Loss of TR without MR Speed Control

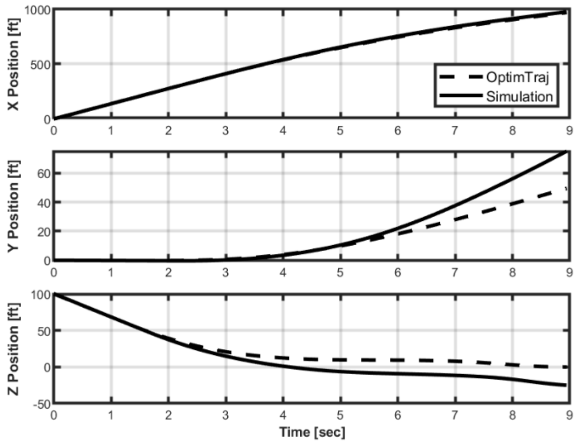

Figure 9. Inertial Positions, Complete Loss of TR without MR Speed Control

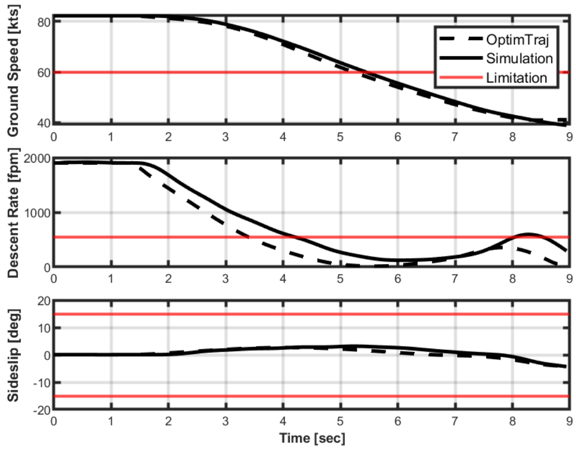

Figure 10. Landing Parameters, Complete Loss of TR without MR Speed Control

5.2. Appendix B: Scenario 2

5.2.1. With MR Speed Control

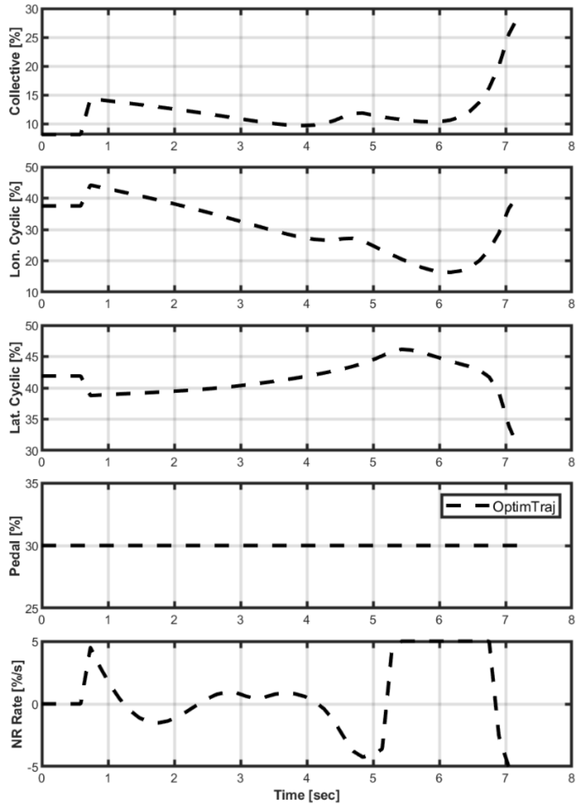

Figure 11. Controls, Pedal Jamming with MR Speed Control

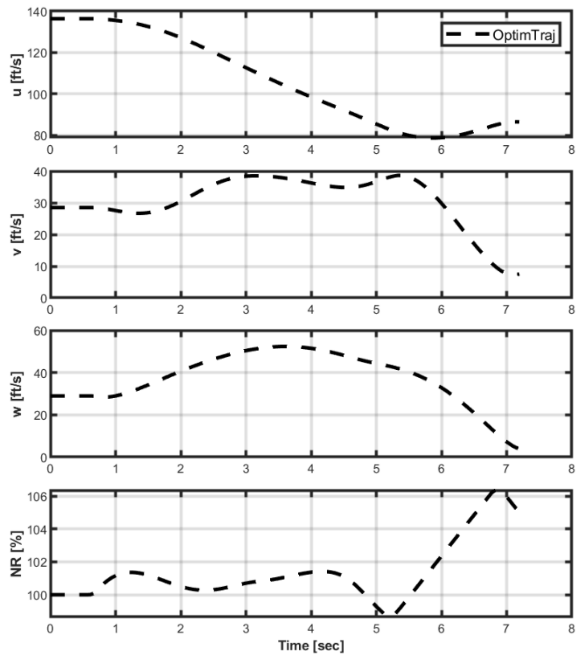

Figure 12. Body Velocities and MR Speed, Pedal Jamming with MR Speed Control

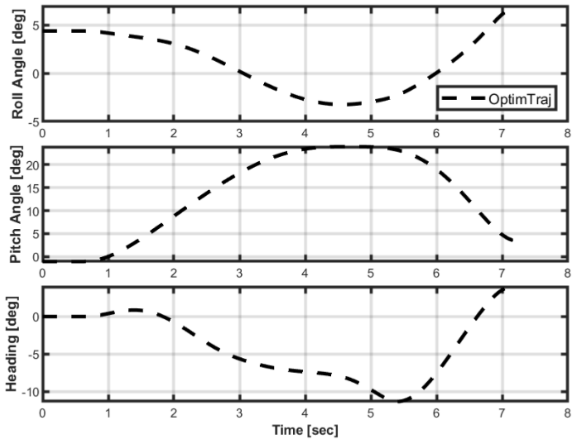

Figure 13. Euler Angles, Pedal Jamming with MR Speed Control

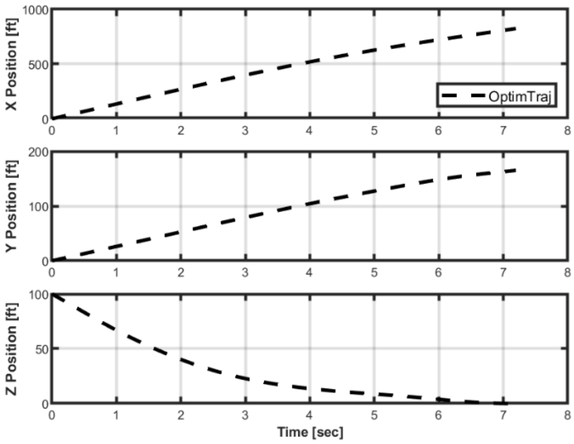

Figure 14. Inertial Position, Pedal Jamming with MR Speed Control

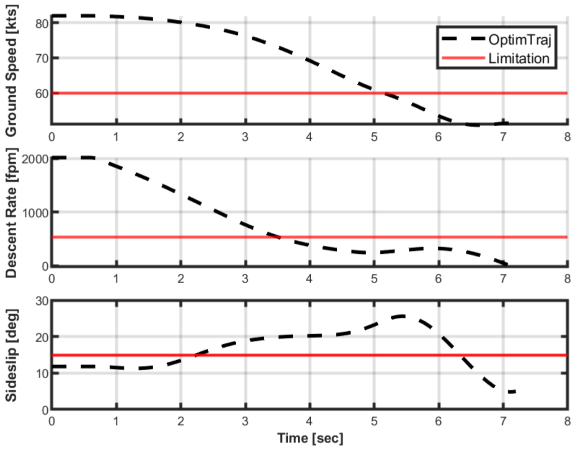

Figure 15. Landing Parameters, Pedal Jamming with MR Speed Control

5.2.2. Without MR Speed Control

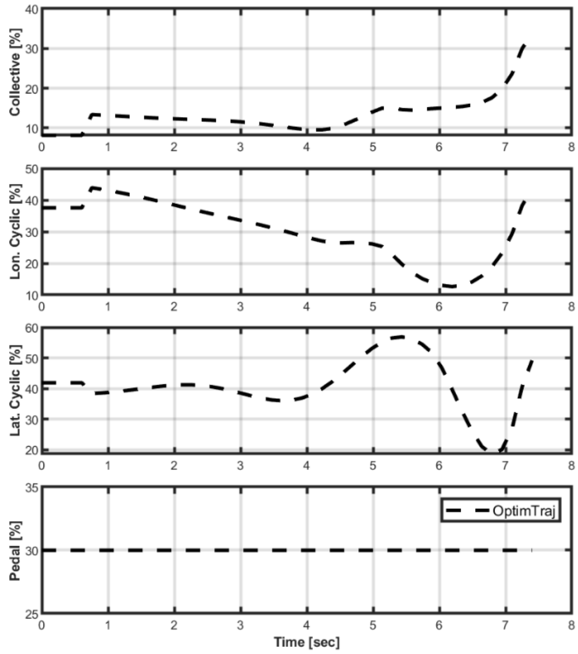

Figure 16. Controls, Pedal Jamming without MR Speed Control

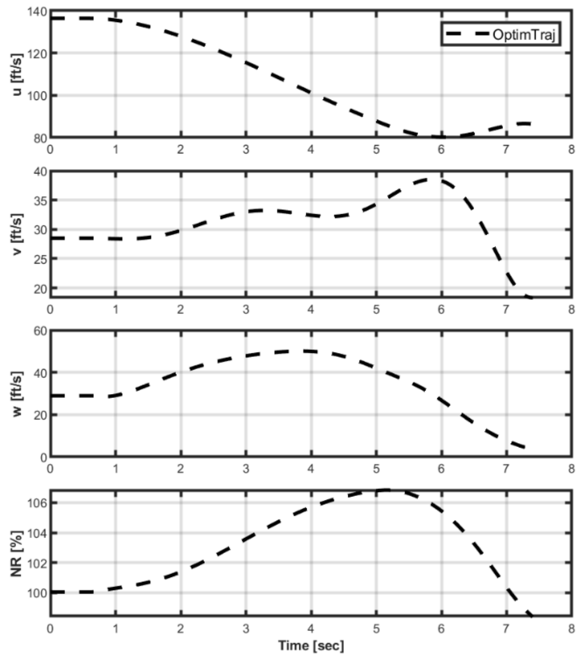

Figure 17. Body Velocities and MR Speed, Pedal Jamming without MR Speed Control

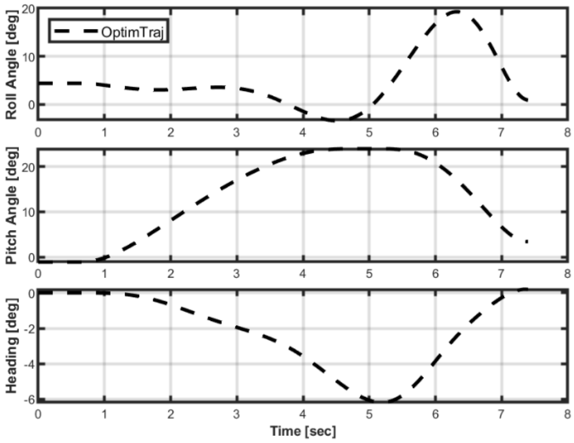

Figure 18. Euler Angles, Pedal Jamming without MR Speed Control

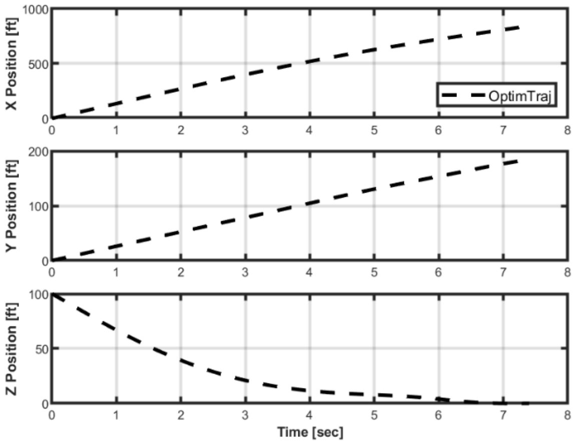

Figure 19. Inertial Positions, Pedal Jamming without MR Speed Control

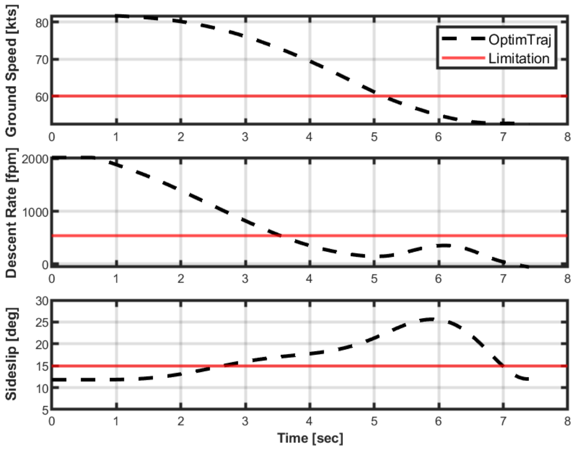

Figure 20, Landing Parameters, Pedal Jamming without MR Speed Control

5.3. Appendix C: Scenario 3

5.3.1. With MR Speed Control

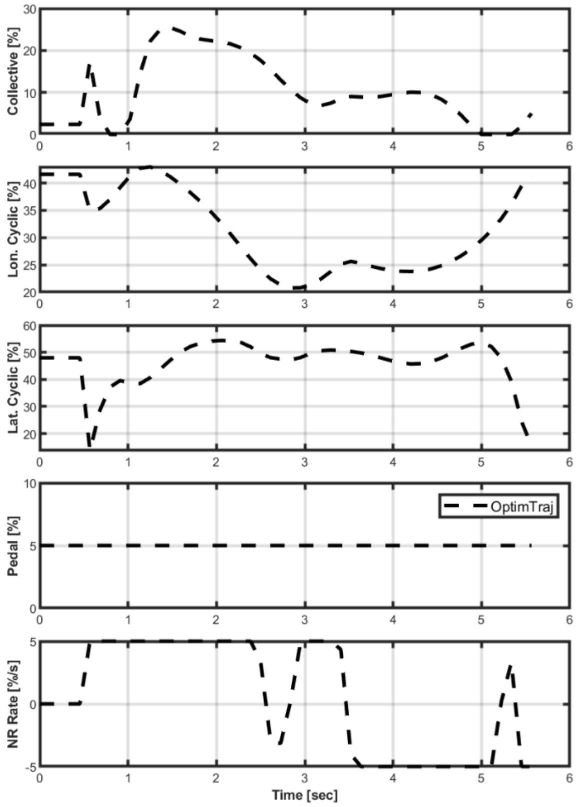

Figure 21. Controls, TR Actuator Hard-Over with MR Speed Control

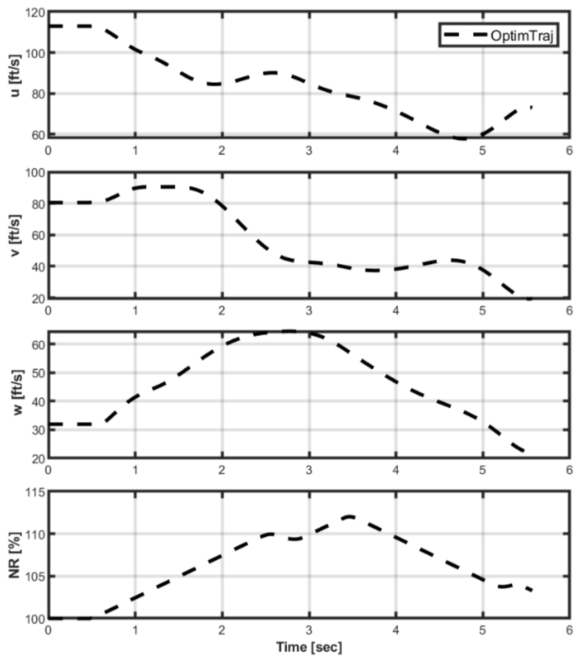

Figure 22. Body Velocities and MR Speed, TR Actuator Hard-Over with MR Speed Control

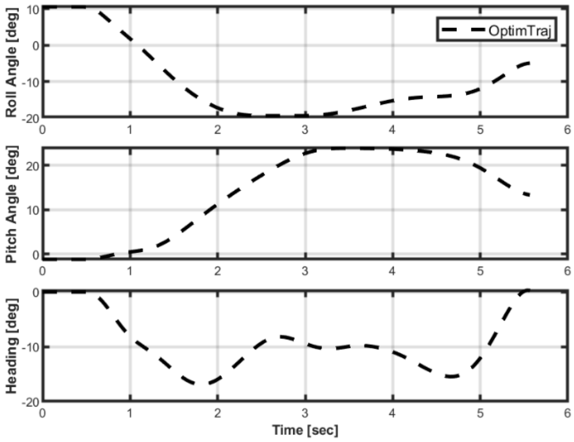

Figure 23. Euler Angles, TR Actuator Hard-Over with MR Speed Control

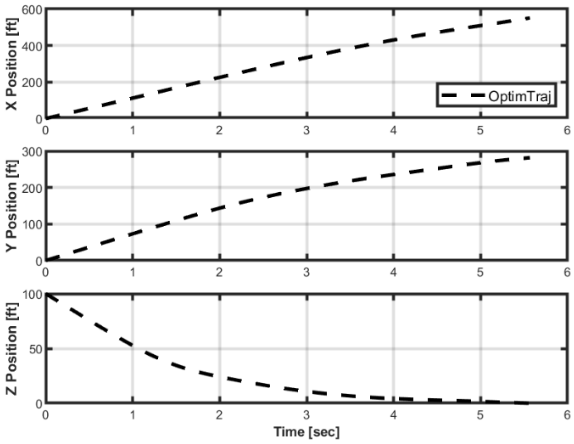

Figure 24. Inertial Positions, TR Actuator Hard-Over with MR Speed Control

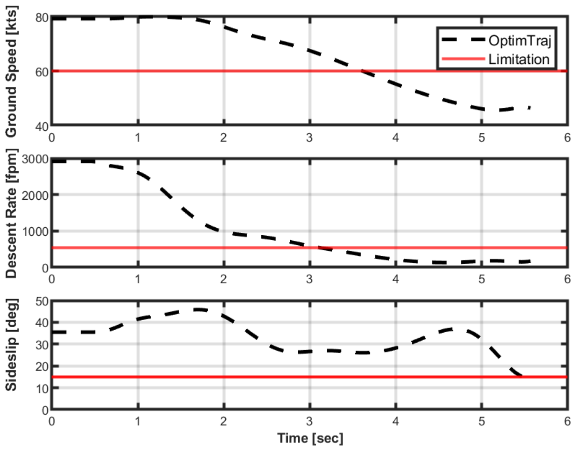

Figure 25. Landing Parameters, TR Actuator Hard-Over with MR Speed Control

5.3.2.Without MR Speed Control

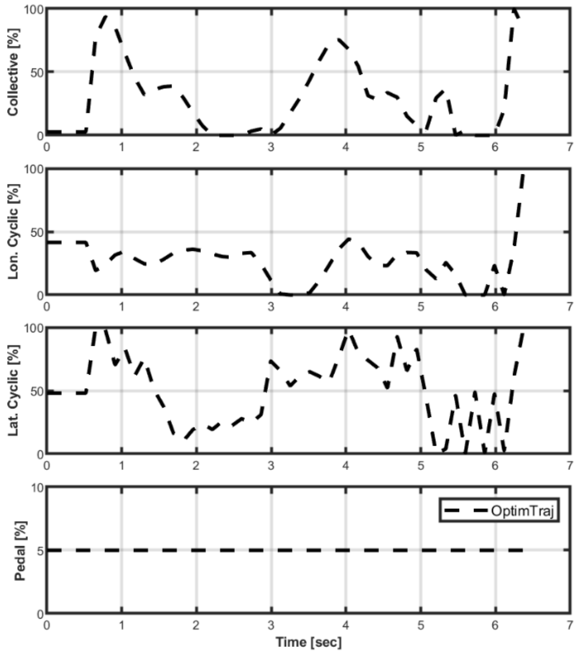

Figure 26. Controls, TR Actuator Hard-Over without MR Speed Control

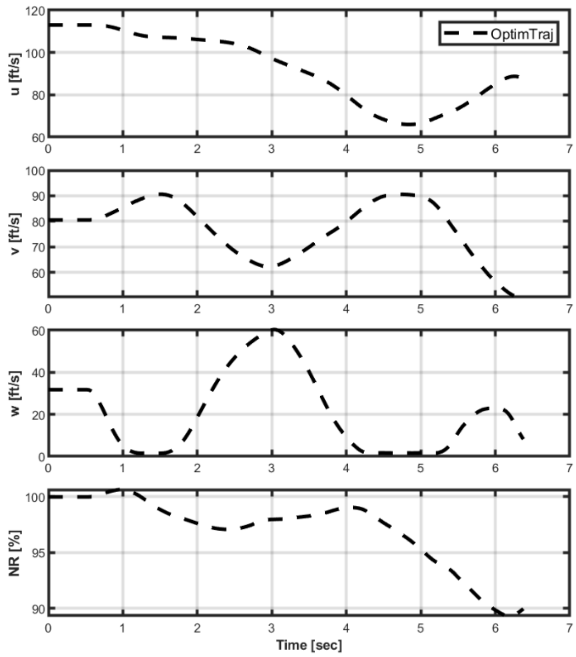

Figure 27. Body Velocities and MR Speed, TR Actuator Hard-Over without MR Speed Control

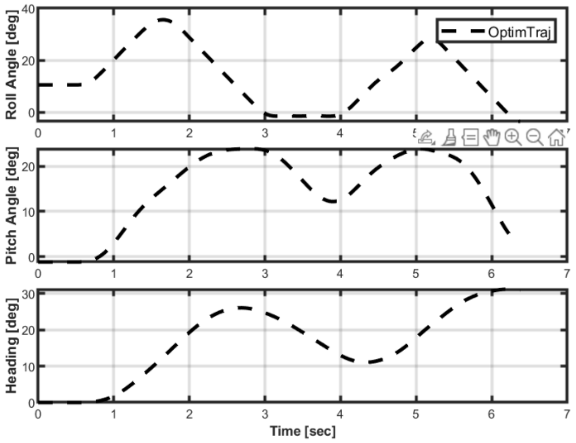

Figure 28. Euler Angles, TR Actuator Hard-Over without MR Speed Control

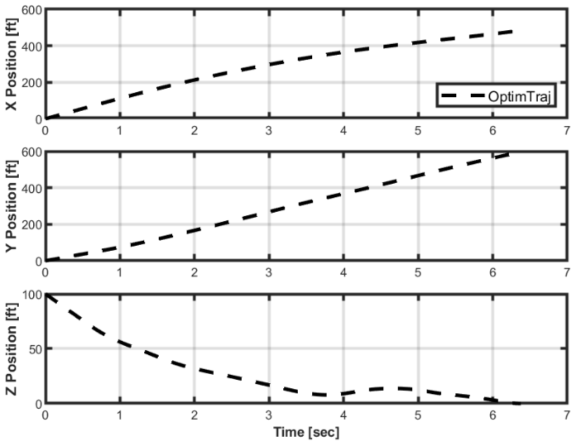

Figure 29. Inertial Positions, TR Actuator Hard-Over without MR Speed Control

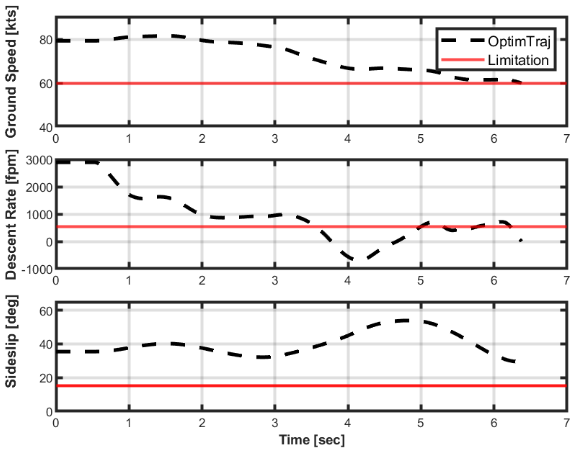

Figure 30. Landing Parameters, TR Actuator Hard-Over without MR Speed Control

6. REFERENCES

1. Australian Transport Safety Bureau, *In-flight tail rotor blade failure and tail assembly separation involving Robinson Helicopter R22, VH-THM.* 2024.

2. Australian Transport Safety Bureau, *Tail rotor driveshaft failure involving Bell Textron 505, VH-VTB.* 2023.

3. U.S. Department of Transportation, Federal Aviation Administration, Flight Standards Service, *Helicopter Flying Handbook,* 2019.

4. Saetti, U., Rogers, J., Alam, M., Jump, M., *Tau Theory-Based Flare Control in Autonomous Helicopter Autorotation*, Aerospace 2024, 11, 33. https://doi.org/10.3390/aerospace11010033

5. Avanzini, G., de Angelis, E. L., de Matteis, G., Fattizzo, D., Giulietti, F., Zavoli, A., *Optimal Trajectory and Tracking Control System for a Helicopter Safe Landing in Autorotation*, 47th European Rotorcraft Forum, United Kingdom, September 7-9, 2021

6. Fattizzo, D. *Attitude and trajectory control system design for the emergency maneuver of a unmanned helicopter*, Alma Mater Studiorum - Università di Bologna, 2024

7. Arslan, Y. O., Okcu, I. D., and Yavrucuk, I., *Flight Path Generation for a Helicopter in Tail Rotor Failure Condition*, 48th European Rotorcraft Forum, Winterthur, Switzerland, September 6-8, 2022

8. Arslan, Y. O., and Okcu, I. D., *Flight Trajectory Tracking for a Helicopter in Tail Rotor Failure*, 49th European Rotorcraft Forum, Bückeburg, Germany, September 5-7, 2023.

9. Arslan, Y. O., Ayık, H. B., and Okcu, I. D., *Control and Navigation of a Helicopter during Tail Rotor Failure*, 50th European Rotorcraft Forum, Marseille, France, September 10-12, 2024

10. Tischler, M. B., Tobias, E. L., *A Model Stitching Architecture for Continuous Full-Flight Envelope Simulation of Fixed Wing Aircraft and Rotorcraft from Discrete-Point Linear Models*, 1 Apr. 2016, U.S. Army AMR-DEC Special Rept. RDMR-AF-16-01.

11. Kelly, M., *An Introduction to Trajectory Optimization: How to Do Your Own Direct Collocation,* SIAM Review, no. 59, pp. 849-904, Jan 2017.

12. Department of the Army, *TM 1-1520-237-10: Operator's Manual for Helicopter, Utility Tactical Transport, UH-60A Black Hawk*, Washington, DC, 2007.

7. CLASSIFICATION & COPYRIGHT

The paper must be unclassified for release to the public and cleared by the appropriate company and/or government agency if necessary. CEAS and its national member societies shall be allowed to publish the paper. The copyright information is stated on the Forum website https://www.rotorcraft-forum.eu/ and on the front page of this template. All papers presented at the ERF will be published as ERF proceedings. In addition they will be available in a freely accessible web-based repository 2 years after the respective conference.